
FOURIER RNNs FOR SEQUENCE PREDICTION

PREPRINT- WORK IN PROGRESS

Moritz Wolter
Institute for Computer Science
University of Bonn
wolter@cs.uni-bonn.de

Angela Yao
School of Computing
National University of Singapore
ayao@comp.nus.edu.sg

March 29, 2022

ABSTRACT

Fourier methods have a long and proven track record as an excellent tool in data processing. We propose to integrate Fourier methods into complex recurrent neural network architectures and show accuracy improvements on prediction tasks as well as computational load reductions. We predict synthetic data drawn from synthetic-equations as well as real world power load data.

1 Introduction

Prior to the popular growth of deep learning approaches, analyzing time series and sequence data in the spectral domain, *i.e.* via a Fourier transform was a standard approach [15, 22, 27]. Fourier analysis separates a time domain signal and represents it as a combination of sinusoids. This can greatly simplify the analysis of recurring superimposed patterns in time series data, since in the spectral domain, the single components become elucidated. In addition, the field of harmonic analysis has the backing of hundreds of years of research in applied mathematics, signal processing, and electrical engineering.

Currently, these advances are not being fully leveraged by the deep learning community. In particular, as recurrent neural networks (RNNs) become the go-to choice for analyzing temporal sequences, it is logical to incorporate Fourier transforms directly into the RNN framework. Doing so not only expands the analysis capabilities of RNNs, but also imparts several computational advantages.

One key problem in the training of recurrent architectures is the difficulty in capturing long-term dependencies of the data in a stable way. Various mitigating approaches exist, with the most common being gating mechanisms as used in LSTMs [19] or GRUs [7]. Alternatives are built around norm preserving weight matrices [3, 20, 39] and there are also hybrids combining gating and norm-preservation [21, 40], though adding a norm-preservation constraint can significantly increase the learning computational cost. While all these approaches help stabilize learning and extend the memory capacity, they do not address the underlying cause of poor long-term memory, which is that RNNs process and learn from only one time step per iteration. Reducing the iterations required to process temporal sequences would be beneficial and complementary to improving the long-term performance of RNNs.

We advocate for integrating the short time Fourier transform (STFT) into RNNs and present in this paper a novel Fourier RNN for analyzing and predicting sequences directly through the frequency domain. In our work, we show that gradients can be back-propagated through the STFT and its inverse. This is especially beneficial for periodic and semi-periodic signals, as they often have informative and compact frequency domain representations. As such, Fourier representations are commonly leveraged for signal processing and recognition [5, 26] as well as compression schemes such as MP3 and JPEG.

The Fourier transform has already been noted in the past for improving the computational efficiency of convolutional neural networks (CNNs) [4, 25, 28, 36, 38]. In CNNs, the efficiency comes from the duality of convolution and multiplication in space versus frequency domains. Fast GPU implementations of convolution, *e.g.* in the NVIDIA cuDNN library [1] use Fourier transforms to speed up their processing. However, the improvement in computational efficiency for our Fourier RNN comes from reductions in data dimensionality and rate in RNN recursion. With the

STFT, we process entire windows of data per RNN step rather than the default single data point, which we find imparts analytical and computational gains.

Since the frequency domain representation is complex-valued, we explore recent advances made in complex-valued networks [35] and specifically complex RNNs [3, 20, 39, 40] to serve as potential foundations for our Fourier RNN. However, our findings show that concatenating the real and imaginary components into one (real-valued) vector is a simple alternative. Our contributions can be summarized as follows:

- We propose a novel RNN architecture for analyzing temporal sequences using the STFT and its inverse; to the best of our knowledge, we are the first to combine STFTs and RNNs into a common framework for sequence prediction.
- We demonstrate how our formulation of the regression problem significantly improves efficiency and can reduce overall training time.
- We demonstrate the strengths of Fourier representations for sequence prediction on synthetic and real-world data and achieve state-of-the-art results on a power load prediction task.

2 Related Works

The analysis of time series in the frequency domain dates back to the early 1800s [17]. Fourier analysis is a staple in a broad swathe of engineering disciplines and is so ubiquitous that the Fast Fourier Transform has been described as the “*most important numerical algorithm of our lifetime*” [33]. In machine learning, Fourier analysis is mostly associated with signal-processing heavy domains such as speech recognition [5], biological signal processing [26], and medical imaging [37] and audio-processing [10, 34]. Recently, a comparison [18] of audio event recognition with neural networks showed the discriminative gains of processing sound in the frequency domain.

The Fourier transform has been used in neural networks in various contexts [16, 41]. Particularly notable are networks, which have Fourier-like units [12, 32] that decompose time series into constituent bases. Within the deep learning community, the discrete Fourier transform has long been touted as a computationally efficient alternative to convolution, since convolution in time and space is equivalent to multiplication in the frequency domain. Such gains are especially relevant for convolutional neural networks in 2D [4, 25, 36, 28] and even more so in 3D [38]. In addition, Fourier-based pooling has been explored for CNNs as an alternative to standard spatial max-pooling [29, 30].

Various methods for adjusting the rate of RNN recurrency have also been explored in the past. One example [24] introduces additional recurrent connections with time lags. Others apply different clock rates to different parts of the hidden layer [2, 23], or apply recursion at multiple (time) scales and or hierarchies [8, 31]. All of these approaches require changes to the basic RNN architecture. Our proposal, however, is an extremely simple alternative which does not require adding any new structures or connections.

3 Short Time Fourier Transform

3.1 Discrete Fourier Transform

The Fourier transform maps a signal into the spectral or frequency domain by decomposing it into a linear combination of periodic waveforms, specifically sinusoids. Analyzing signals in the spectral domain with the Fourier transform is a fundamental tool in engineering [27]. For the uninitiated reader, the discrete Fourier transform \mathcal{F} for a (discrete) signal \mathbf{x} is defined as

$$\mathbf{X}[\omega] = \mathcal{F}(\mathbf{x}) = \sum_{l=-\infty}^{\infty} \mathbf{x}[l]e^{-j\omega l}, \quad (1)$$

where l is the (time) signal index¹, ω denotes the frequency, e the exponential function and $j = \sqrt{-1}$. As such, the Fourier transform $\mathbf{X}[\omega]$ is complex-valued, *i.e.* $\mathbf{X}[\omega] \in \mathbb{C}$.

One can recover the signal $\hat{\mathbf{x}}$ from \mathbf{X} by taking the inverse discrete Fourier transform \mathcal{F}^{-1} , *i.e.*

$$\hat{\mathbf{x}}[l] = \mathcal{F}^{-1}(\mathbf{x}) = \sum_{l=-\infty}^{\infty} \mathbf{X}[l]e^{j\omega l}, \quad (2)$$

¹For convenience, we refer to the signal index interchangeably as time, though l can denote any other evenly spaced signal index as well.

3.2 Forwards STFT

Note that the definition of the Fourier transform in Eq. 1 requires infinite support of the time signal to estimate the frequency response. For many real-world applications, however, including those which we wish to model with RNNs, this requirement is not only infeasible, but also necessary to obtain insights into changes in the frequency spectrum as function of time or signal index. To do so, one can partition the signal into overlapping segments and approximating the Fourier transform of each segment separately. This is the core idea behind the short time Fourier transform (STFT), which is used to determine a signal's frequency domain representations as it changes over time.

More formally, given a signal \mathbf{x} , we can partition it into segments of length T , extracted every S time steps. The STFT \mathcal{F}_s of \mathbf{x} is defined by [9] as the discrete Fourier transform of \mathbf{x} , *i.e.*

$$\mathbf{X}[\omega, Sm] = \mathcal{F}_s(\mathbf{x}) = \mathcal{F}(\mathbf{w}[Sm - l]\mathbf{x}[l]) = \sum_{l=-\infty}^{\infty} \mathbf{w}[Sm - l]\mathbf{x}[l]e^{-j\omega l}, \quad (3)$$

we observe that segments of \mathbf{x} are multiplied with the windowing function \mathbf{w} and transformed afterwards. It follows an implementation of Eq. 3 by taking the fast Fourier Transform (FFT) of a signal segment \mathbf{x}_s multiplied by the window \mathbf{w} .

3.3 Windowing

In working with the STFT, the main parameters to consider are the shape and effective width of the windowing function \mathbf{w} as given in Eq. 3. The simplest windowing function is a rectangle, and simply extracts the signal \mathbf{x} in its original form. However, the sharp drop-off at the edge of a rectangular window requires infinite spectral support and as such results in more spectrum leakage of \mathbf{X} in the frequency domain². As such, smooth “bell”-shaped functions such as Hanning or Gaussians windows (see Fig.1) are recommended instead [13]. Note that having such windows does not reduce leakage persay – it simply allows for a different distribution of the leakage.

The width of the window determines the resolution in which the signal \mathbf{x} is represented. Wide windows offer high frequency resolution, but as a result, lose out on resolution temporally. On the other hand, narrow windows which offer better temporal resolution have poor frequency resolution. The choice in window width trades off between the two and should be chosen depending on the application at hand.

3.4 Inverse STFT

Supposing that we are given some frequency signal \mathbf{X} ; the time signal $\hat{\mathbf{x}}$ represented by \mathbf{X} can be recovered with the inverse short time Fourier transform (iSTFT) \mathcal{F}_s^{-1} and is defined by [9] as:

$$\hat{\mathbf{x}}[n] = \mathcal{F}_s^{-1}(\mathbf{X}[n, Sm]) = \frac{\sum_{m=-\infty}^{\infty} \mathbf{w}[Sm - n]\hat{\mathbf{x}}_w[n, Sm]}{\sum_{m=-\infty}^{\infty} \mathbf{w}^2[Sm - n]}, \quad (4)$$

where the signal $\hat{\mathbf{x}}_w$ is the inverse Fourier transform of \mathbf{X} :

$$\hat{\mathbf{x}}_w = \frac{1}{T} \sum_{l=-\infty}^{\infty} \mathbf{X}[l, Sm]e^{j\omega l}, \quad (5)$$

and l indexing the frequency dimension of \mathbf{X}_m .

Eq. 4 reverses the effect of the windowing function, but implementations require careful treatment of the denominator to prevent division by near-zero values³. In Eq. 4, Sm generally evaluates to an integer smaller than the window size T and subsequent elements in the sum overlap, hence the alternative naming of it being an “*overlap and add*” method [13].

²Multiplication with the window function in the time domain is equivalent to convolution with its Fourier transform in the frequency or spectral domain; as such, the wider the spectral response of the window function, the greater the spread and blurring of the frequency response of the original signal.

³We adopt the common strategy of adding a small tolerance $\epsilon = 0.001$

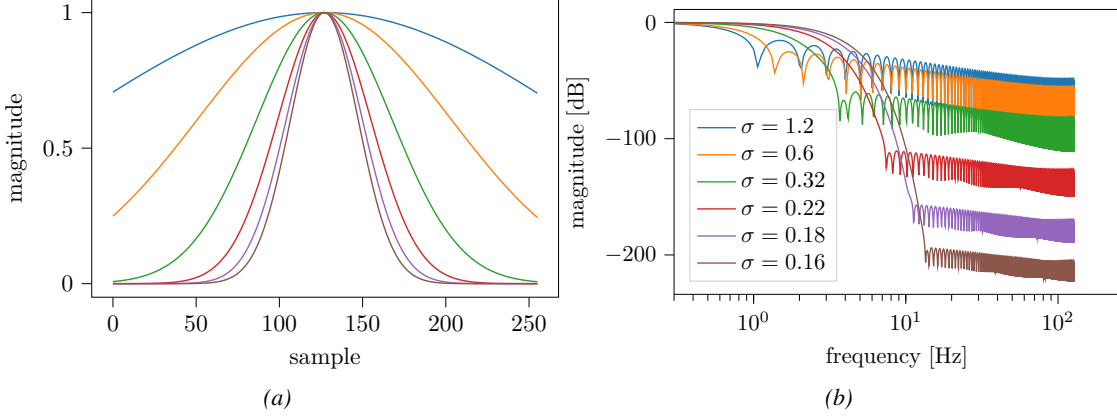


Figure 1: (a) Gaussian window with varying standard deviation $\sigma \in [0, \infty)$. (b) Fourier transform of Gaussian window

4 Fourier Recurrent Neural Networks

4.1 Basic RNN

We begin by defining a real-valued basic recurrent neural network (RNN) as follows:

$$\mathbf{z}_t = \mathbf{W}\mathbf{h}_{t-1} + \mathbf{V}\mathbf{x}_t + \mathbf{b} \quad (6)$$

$$\mathbf{h}_t = f_a(\mathbf{z}_t) \quad (7)$$

$$\mathbf{y}_t = \mathbf{W}_p\mathbf{h}_t \quad (8)$$

The input, hidden unit and output vectors are given respectively by $\mathbf{x}_t \in \mathbb{R}^{1 \times 1}$, $\mathbf{h}_t \in \mathbb{R}^{n_h \times 1}$ and $\mathbf{y}_t \in \mathbb{R}^{n_y \times 1}$ at time t , where n_x , n_h and n_y are the dimensionalities of the input, hidden and output states respectively. The function f_a is a non-linear activation; hyperbolic tangents are a common choice for RNNs. The network weights are defined as real-valued matrices, *i.e.* $\mathbf{W} \in \mathbb{R}^{n_h \times n_h}$, $\mathbf{V} \in \mathbb{R}^{n_h \times n_x}$, $\mathbf{b} \in \mathbb{R}^{n_h \times 1}$ and $\mathbf{W}_p \in \mathbb{R}^{n_h \times n_y}$.

4.2 Fourier RNN

We can move RNN processing into the frequency domain and define our Fourier RNN (fRNN) by applying the STFT to the input signal x . If the output or projection of the final hidden vector is also a signal of the temporal domain, we can also apply the iSTFT to recover the output y . This can be summarized by the following set of RNN equations:

$$\mathbf{X}_\tau = \mathcal{F}(\{\mathbf{x}_{S\tau-T/2}, \dots, \mathbf{x}_{S\tau+T/2}\}) \quad (9)$$

$$\mathbf{z}_\tau = \mathbf{W}_c\mathbf{h}_{\tau-1} + \mathbf{V}_c\mathbf{X}_\tau + \mathbf{b}_c \quad (10)$$

$$\mathbf{h}_\tau = f_a(\mathbf{z}_\tau) \quad (11)$$

$$\mathbf{y}_\tau = \mathcal{F}^{-1}(\{\mathbf{W}_{pc}\mathbf{h}_0, \dots, \mathbf{W}_{pc}\mathbf{h}_\tau\}) \quad (12)$$

where $\tau = [0, n_s]$, *i.e.* from zero to the total number of segments n_s . The output y_τ may be computed based on the available outputs $\{\mathbf{W}_p\mathbf{h}_0, \dots, \mathbf{W}_p\mathbf{h}_\tau\}$ at step τ .

Note that even though equations 10 to 12 are exactly analogous to the basic RNN in equations 6 to 8, the change from \mathbf{x}_t to \mathbf{X}_τ has two key implications. First of all, because $\mathbf{X}_\tau \in \mathbb{C}^{n_f \times 1}$ is a complex signal, the hidden state as well as subsequent weight matrices all become complex, *i.e.* $\mathbf{h}_\tau \in \mathbb{C}^{n_h \times 1}$, $\mathbf{W}_c \in \mathbb{C}^{n_h \times n_h}$, $\mathbf{V}_c \in \mathbb{C}^{n_h \times n_f}$, $\mathbf{b}_c \in \mathbb{C}^{n_h \times 1}$ and $\mathbf{W}_{pc} \in \mathbb{C}^{n_h \times n_f}$, where n_h is the hidden size of the networks as before and n_f is the number of frequencies in the STFT.

The second implication to note is that the step index in the fRNN, by changing from t to τ , means that the fRNN effectively covers S time steps of the standard RNN per step. This has significant bearing on the overall memory consumption as well as the computational cost, both of which influence the overall network training time.

Considering only the multiplication of the state matrix \mathbf{W}_c and the state vector \mathbf{h}_τ , which is the most expensive operation, the basic RNN requires $N \cdot O(n_h^3)$ operations for N total time steps. When using the Fourier RNN with an FFT implementation of the STFT, one requires only

$$N/S \cdot (O(T \log T) + O(n_h^3)), \quad (13)$$

where the $T \log T$ term comes from the FFT operation. The architectural changes lead to larger input layers and fewer RNN iterations. \mathbf{X} is higher dimensional than \mathbf{x} , but we save on overall computation as the step size is large enough which will make N/S much smaller than N .

We can generalise the approach described above into:

$$\mathbf{X}_\tau = \mathcal{F}(\{\mathbf{x}_{S\tau-T/2}, \dots, \mathbf{x}_{S\tau+T/2}\}) \quad (14)$$

$$\mathbf{h}_t = \text{RNN}_\mathbb{C}(\mathbf{X}_\tau, \mathbf{h}_{t-1}) \quad (15)$$

$$\mathbf{y}_t = \mathcal{F}^{-1}(\{\mathbf{W}_{pc}\mathbf{h}_0, \dots, \mathbf{W}_{pc}\mathbf{h}_\tau\}), \quad (16)$$

where instead of the basic formulation outlined above, more sophisticated complex-valued RNN-architectures [3, 39, 40] represented by $\text{RNN}_\mathbb{C}$ may be substituted. Our preliminary experiments with a complex-valued GRU, as proposed in [40] show marginally better performance though at significantly more computational expense, due to the extra calculations required in the complex-valued non-linearity. As such, we simply concatenate the real and imaginary components into one (real-valued) hidden vector and report results based on such a work-around for the rest of this paper.

4.3 Window Selection

Historically, the shape and width of the window function have been selected by hand. We work with an adjustable window and fix the parameterization as a part of the learning process. Out of simplicity, we choose a truncated Gaussian [14], where σ , the standard deviation of the Gaussian, controls the extent of tapering as well as window width. The larger that σ is, the more the window function approaches a rectangular window; the smaller the sigma, the more extreme the edge tapering and as a result, the narrower the window width. Fig. 1 illustrates the different windows (a) and their corresponding frequency domain response (b).

5 Mackey-Glass Experiments

We first study our method by applying it to make predictions on the Mackey-Glass series [11]. The Mackey-Glass equation is a non-linear time-delay differential and defines a chaotic system that is semi-periodic:

$$\frac{dx}{dt} = \frac{\beta x_\tau}{1 + x_\tau^n} - \gamma x, \quad (17)$$

with $\gamma = 0.1, \beta = 0.2$ and $n = 10$. x_τ evaluates as the value from τ time steps ago; we use a delay of $\tau = 17$ and simulate the equation in the interval $t \in [0, 512]$ using a forward Euler scheme with a time step of size 0.1. During the warm-up, when true values are not yet known, we randomly draw values from $1 + U[-0.1, 0.1]$. An example of the time series can be found in Fig. 2 (a); we split the signal in half, conditioning on the first half as input and predict the second half.

In all experiments, we use RNN architectures based on GRU-cells [6] with a state size of 64 and a Gaussian window of width 128 initialized at $\sigma = 0.5$ unless otherwise stated. The learning rate was set initially to 0.001 and then reduced with a stair-wise exponential decay with a decay rate of 0.9 every 1000 steps. Training was stopped after 20000 steps.

5.1 Chaotic Sequence Prediction

We compare against two time-based lines: a standard GRU (time-RNN) and a windowed version (time-RNN windowed) in which we reshape the input and process windows of data together instead of single scalars. This effectively sets the clock rate of the RNN to be per window rather than per time step. As comparison, we look at our Fourier RNN as described in section 4.2 (fRNN) with a GRU-cell and a low-pass filtered version keeping only the first four coefficients (fRNN lowpass). For all four networks, we use a fixed hidden-state size of 64, which results in networks with 13k, 29k, 46k and 14k parameters for the time-RNN, time-windowed RNN, fRNN and lowpass fRNN respectively.

From Fig. 2(a), we observe that all four architecture variants are able to predict the overall time series trajectory, though the time-windowed RNN and the standard fRNN suffer from high-frequency noise (see close-up in Fig. 2 (b)). The standard time-based RNN and the low-pass filtered RNN, however, maintain smooth time-series trajectories. Quantitatively, we see from Fig. 2(c) that our fRNN method has a much lower MSE than the time-based approaches. The time-based RNN struggles with processing and retaining all of the contextual points in the memory and as a result, has the highest MSE.

Looking at the learning behaviour in Fig. 2 (c), we observe that the windowed networks, both in time and in the Fourier RNNs converge much faster than the standard time-based RNN. This difference becomes especially pronounced if

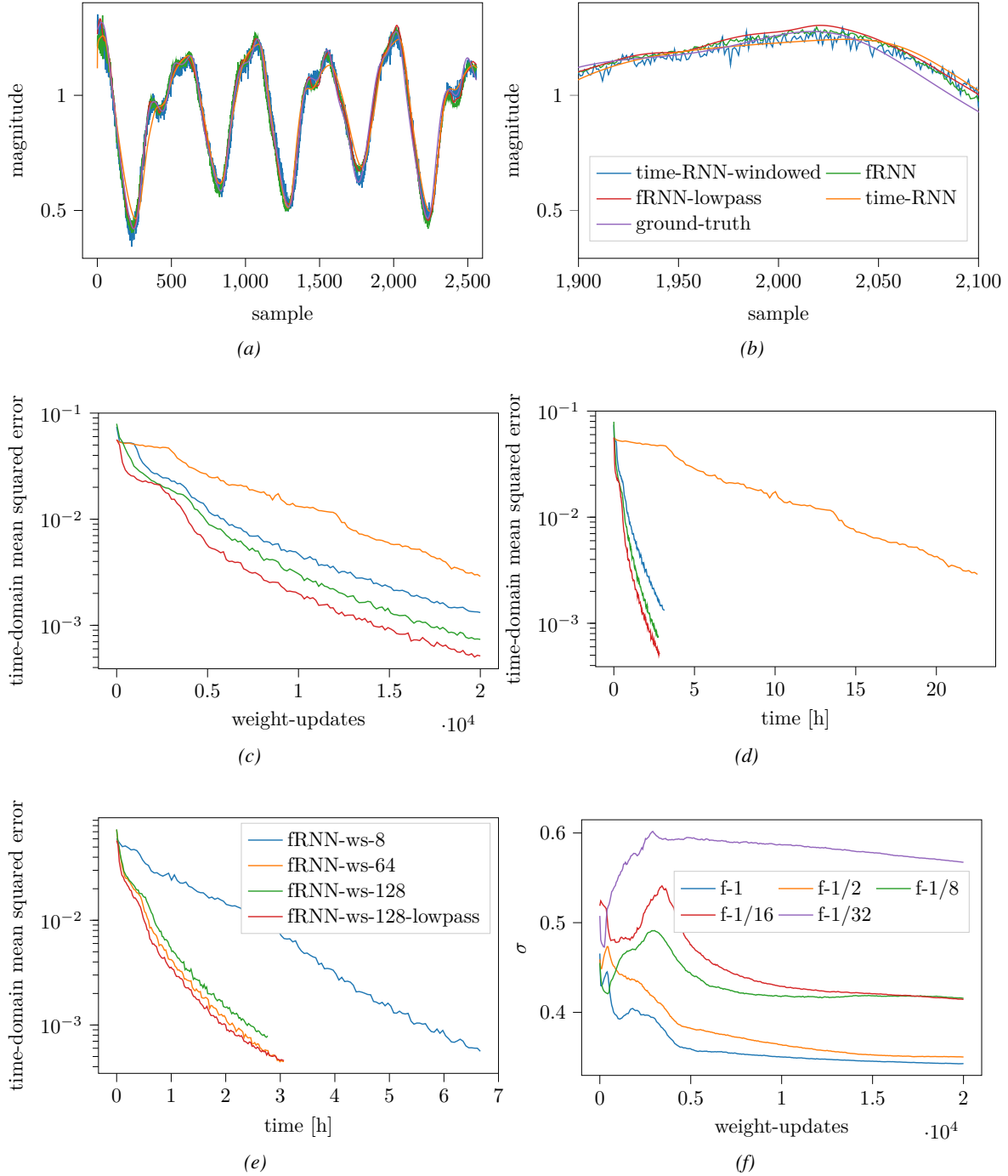


Figure 2: Mackey-Glass series predictions in (a) for different RNN methods. The close-up in (b) shows that the time-RNN and the low-pass filtered fRNN maintain smooth and coherent time series predictions, while the time-windowed RNN and standard fRNN suffers from high-frequency noise, even though it also successfully recovers the overall trajectory of the time series. The mean squared error of the different methods are shown over weight updates (c) and runtime (d). (e) plots error and runtime for experiments with increasing window size. (f) shows the learned window width for increasing degrees of low-pass filtering. Figure best viewed in colour. The legend in (b) applies in (a), (c) and (d) as well.

Table 1: Real and complex valued architecture comparison on the mackey-glass data.

net	weights	mse	time [min]
gru-64-fft	46k	$7.4 \cdot 10^{-4}$	172
cgRNN-32-fft	23k	$9.3 \cdot 10^{-4}$	275
cgRNN-54-fft	46k	$5.2 \cdot 10^{-4}$	230
cgRNN-64-fft	58k	$3.4 \cdot 10^{-4}$	272

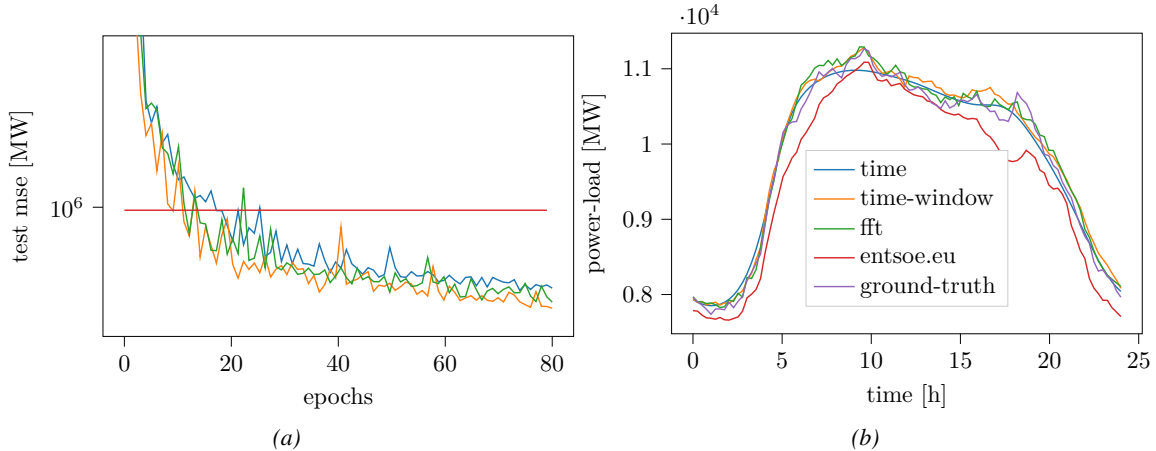


Figure 3: Day ahead prediction results. We observe that all deep learning approaches beat the entsoe.eu baseline, which suggests that their approach could benefit from deep learning.

one factors in the number of computations (and therefore time) per weight update, as discussed in Eq. 13. This result is shown in Fig. 2(d); both Fourier RNNs as well as the time-windowed baseline require less than one-sixth of the computation time and still converge to lower MSE values. We explore the effect of the window width in Fig. 2(e). We observe a reduction in run-time coupled with an initial reduction in error. When the window size increases high frequency noise starts to appear, this effect is visible in Figure 2(e), we counteract this phenomenon using low-pass filtering. The filtering affects the width of the window function kernel. Figure 2(e) illustrates this effect. Increasing low-pass filtering rates are shown, for more aggressive filtering the optimizer chooses a wider kernel.

We explore the effect of a complex valued cell in table 1. We apply the complex gru proposed in [40], and compare to a real valued gru. We speculate that complex cells are better suited to process fourier representations due to their complex nature. Our observations show that both cells solve the task, while the complex cell does so with fewer parameters at a higher cost.

6 Power Load Forecasting

We apply our Fourier RNN to the problem of forecasting power consumption since power load data has periodic behaviour with respect to time. We use the power load data of 36 EU countries from 2011 to 2019 as provided by the European Network of Transmission System Operators for Electricity⁴. We partition the data into two groups; those reporting with a 15 minute frequency are used for day-ahead predictions, while those with hourly reports are used for longer-term predictions. For testing we hold back the German Tennet load recordings from 2015, all of Belgiums recordings of 2016, Austrias load of 2017 and finally the consumption of the German Ampiron grid in 2018. An example plot of the data and its autocorrelation function is shown shown in the supplementary material.

We start with the task of day-ahead prediction; using 14 days of context, at 12:00, we are asked to predict 24 hours of load from midnight onwards. We do this by prediction the load from noon until midnight on the prediction day plus the next day and ignore the values from the prediction day. During training, the initial learning rate was set to 0.004 and exponentially decayed using a decay of 0.95 every epoch. We train for 80 epochs overall. We compare time domain,

⁴<https://transparency.entsoe.eu/>; for reproducibility, we have added a compressed version of the data to the supplementary material and will release it online upon paper acceptance.

Table 2: 60 day ahead power load prediction and ground truth. Power prediction results using various different architectures

Network	mse [MW]	weights	run [min]
time-RNN	$1.3 \cdot 10^7$	13k	772
time-RNN-windowed	$8.8 \cdot 10^5$	28k	12
fRNN	$8.3 \cdot 10^5$	44k	13
fRNN-lowpass-1/4	$7.6 \cdot 10^5$	20k	13
fRNN-lowpass-1/8	$1.3 \cdot 10^6$	16k	13

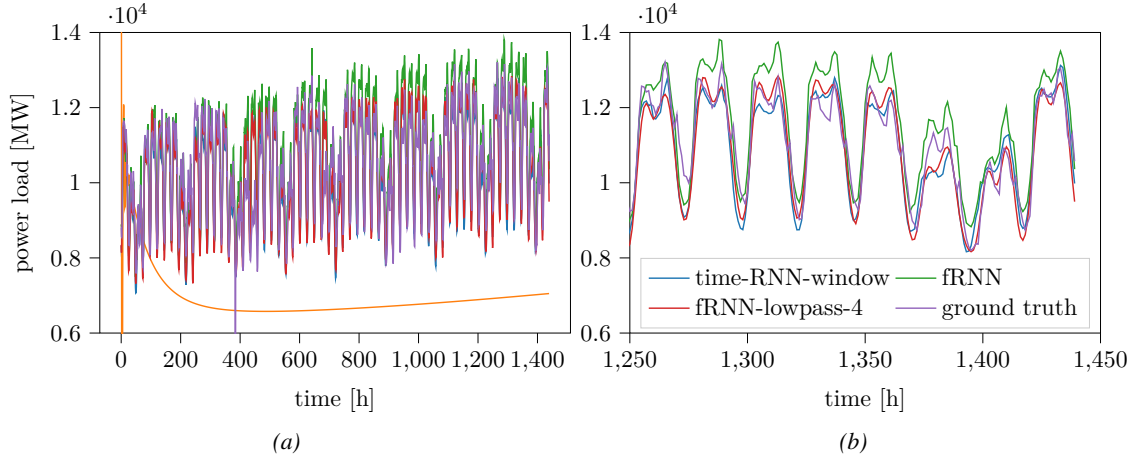


Figure 4: A test set sample for showing the 60 day prediction results for all architectures under consideration. The full signal (a) as well as only the last week (b). The time-RNN prediction is shown in yellow.

windowed time as well as windowed Fourier approaches. The window size was set to 96 which corresponds to 24 hours of data at a sampling rate of 15 minutes per sample.

In figure 3 we observe that all approaches we tried produce reasonable solutions and outperform the prediction produced by the European Network of Transmission System Operators for Electricity which suggests that their approach could benefit from deep learning.

Next we consider the more challenging task of 60 day load prediction using 120 days of context. We use 12 load samples per day from all entenso-e member states from 2015 until 2019. We choose a window size of 120 samples or five days; all other parameters are left the same as the day-ahead prediction setting. Table 2 shows that the windowed methods are able to extract patterns, but the scalar-time domain approach failed. Additionally we observe that we do not require the full set of Fourier coefficients to construct useful predictions on the power-data set. The results are tabulated in table 2. It turns out that the lower quarter of Fourier coefficients is enough, which allowed us to reduce the number of parameters considerably.

7 Conclusion

In this paper, we have proposed to integrate the Short Time Fourier transform and it’s inverse into RNN architectures and evaluated the performance of real and complex valued cells in this setting. The resulting Fourier RNNs allow us to efficiently compute long high resolution predictions for both real and synthetic periodic or quasi-periodic time series. Reducing the clock rate of the RNN leads to substantial computational savings while low pass filtering allows us to keep the parameter growth from the windowing under control.

References

- [1] NVIDIA Developer Fourier transforms in convolution. <https://developer.nvidia.com/discover/convolution>. Accessed: 2019-05-09.
- [2] Tayfun Alpay, Stefan Heinrich, and Stefan Wermter. Learning multiple timescales in recurrent neural networks. In *International Conference on Artificial Neural Networks*, pages 132–139. Springer, 2016.
- [3] M. Arjovsky, A. Shah, and Y. Bengio. Unitary evolution recurrent neural networks. In *ICML*, 2016.
- [4] Yoshua Bengio, Yann LeCun, et al. Scaling learning algorithms towards ai. *Large-scale kernel machines*, 34(5):1–41, 2007.
- [5] William Chan, Navdeep Jaitly, Quoc Le, and Oriol Vinyals. Listen, attend and spell: A neural network for large vocabulary conversational speech recognition. In *Acoustics, Speech and Signal Processing (ICASSP), 2016 IEEE International Conference on*, pages 4960–4964. IEEE, 2016.
- [6] K. Cho, B. van Merriënboer, Ç. Gülçehre, D. Bahdanau, F. Bougares, H. Schwenk, and Y. Bengio. Learning phrase representations using RNN encoder–decoder for statistical machine translation. In *EMNLP*, 2014.
- [7] Kyunghyun Cho, Bart van Merriënboer, Çağlar Gülçehre, Dzmitry Bahdanau, Fethi Bougares, Holger Schwenk, and Yoshua Bengio. Learning phrase representations using rnn encoder-decoder for statistical machine translation. In *EMNLP*, 2014.
- [8] Junyoung Chung, Sungjin Ahn, and Yoshua Bengio. Hierarchical multiscale recurrent neural networks. In *ICLR*, 2017.
- [9] J. Lim D. Griffin. Signal estimation from modified short-time fourier transform. In *IEEE Transactions on Acoustics, Speech, and Signal Processing*, 1984.
- [10] Sander Dieleman and Benjamin Schrauwen. End-to-end learning for music audio. In *Acoustics, Speech and Signal Processing (ICASSP), 2014 IEEE International Conference on*, pages 6964–6968. IEEE, 2014.
- [11] Felix A Gers, Douglas Eck, and Jürgen Schmidhuber. Applying lstm to time series predictable through time-window approaches. In *Neural Nets WIRN Vietri-01*, pages 193–200. Springer, 2002.
- [12] L. B. Godfrey and M. S. Gashler. Neural decomposition of time-series data for effective generalization. *IEEE Transactions on Neural Networks and Learning Systems*, 29(7):2973–2985, July 2018.
- [13] Karlheinz Gröchenig. *Foundations of time-frequency analysis*. Springer Science & Business Media, 2013.
- [14] Fredric J Harris. On the use of windows for harmonic analysis with the discrete fourier transform. *Proceedings of the IEEE*, 66(1):51–83, 1978.
- [15] William Hayt, Jack E. Kemmerly, and Steven M. Durbin. *Engineering Circuit Analysis*. McGraw-Hill Education - Europe, 2011.
- [16] Robert Hecht-Nielsen. Theory of the backpropagation neural network. In *Neural networks for perception*, pages 65–93. Elsevier, 1992.
- [17] Michael Heideman, Don Johnson, and C Burrus. Gauss and the history of the fast fourier transform. *IEEE ASSP Magazine*, 1(4):14–21, 1984.
- [18] Lars Hertel, Huy Phan, and Alfred Mertins. Comparing time and frequency domain for audio event recognition using deep learning. In *Neural Networks (IJCNN), 2016 International Joint Conference on*, pages 3407–3411. IEEE, 2016.
- [19] S. Hochreiter and J. Schmidhuber. Long short term memory. *Neural Computation*, 1997.
- [20] S. Hyland and G. Rätsch. Learning unitary operators with help from $u(n)$. In *AAAI*, 2017.
- [21] L. Jing, C. Gulcehre, J. Peurifoy, Y. Shen, M. Tegmark, M. Solja, and Y. Bengio. Gated orthogonal recurrent units: On learning to forget. In *AAAI Workshops*, 2018.
- [22] Viloms Komornik and Paola Loretì. *Fourier Series in Control Theory*. Springer Monographs in Mathematics, 2005.
- [23] Jan Koutník, Klaus Greff, Faustino Gomez, and Juergen Schmidhuber. A clockwork rnn. In *International Conference on Machine Learning*, pages 1863–1871, 2014.
- [24] Tsungnan Lin, Bill G Horne, Peter Tino, and C Lee Giles. Learning long-term dependencies in narx recurrent neural networks. *IEEE Transactions on Neural Networks*, 7(6):1329–1338, 1996.
- [25] Michael Mathieu, Mikael Henaff, and Yann LeCun. Fast training of convolutional networks through ffts. *arXiv preprint arXiv:1312.5851*, 2013.
- [26] K. Minami, H. Nakajima, and T. Toyoshima. Real-time discrimination of ventricular tachyarrhythmia with fourier-transform neural network. *IEEE Transactions on Biomedical Engineering*, 46(2):179–185, Feb 1999.
- [27] Rik Pintelon and Johan Schoukens. *System identification: A frequency domain approach*. John Wiley & Sons, 2012.
- [28] Harry Pratt, Bryan Williams, Frans Coenen, and Yalin Zheng. FCNN: fourier convolutional neural networks. In *Joint European Conference on Machine Learning and Knowledge Discovery in Databases*, pages 786–798. Springer, 2017.
- [29] Oren Rippel, Jasper Snoek, and Ryan P Adams. Spectral representations for convolutional neural networks. In *Advances in neural information processing systems*, pages 2449–2457, 2015.

- [30] Jongbin Ryu, Ming-Hsuan Yang, and Jongwoo Lim. Dft-based transformation invariant pooling layer for visual classification. In *ECCV*, 2018.
- [31] Iulian Vlad Serban, Tim Klinger, Gerald Tesauro, Kartik Talamadupula, Bowen Zhou, Yoshua Bengio, and Aaron Courville. Multiresolution recurrent neural networks: An application to dialogue response generation. In *Thirty-First AAAI Conference on Artificial Intelligence*, 2017.
- [32] Adrian Silvescu. Fourier neural networks. In *IJCNN'99. International Joint Conference on Neural Networks. Proceedings (Cat. No. 99CH36339)*, volume 1, pages 488–491. IEEE, 1999.
- [33] Gilbert Strang. Wavelets. *American Scientist*, 82(3):250–255, 1994.
- [34] J. Thickstun, Z. Harchaoui, and S.M. Kakade. Learning features of music from scratch. In *ICLR*, 2017.
- [35] C. Trabelsi, O. Bilaniuk, Y. Zhang, D. Serdyuk, S. Subramanian, J. F. Santos, S. Mehri, N. Rostamzadeh, Y. Bengio, and C.J. Pal. Deep complex networks. In *ICLR*, 2018.
- [36] Nicolas Vasilache, Jeff Johnson, Michael Mathieu, Soumith Chintala, Serkan Piantino, and Yann LeCun. Fast convolutional nets with fbfft: A GPU performance evaluation. In *ICLR*, 2015.
- [37] P. Virtue, S.X. Yu, and M. Lustig. Better than real: Complex-valued neural nets for MRI fingerprinting. In *ICIP*, 2017.
- [38] Zelong Wang, Qiang Lan, Hongjun He, and Chunyuan Zhang. Winograd algorithm for 3D convolution neural networks. In *ICANN*, 2017.
- [39] S. Wisdom, T. Powers, J.R. Hershey, J. Le Roux, , and L. Atlas. Full-capacity unitary recurrent neural networks. In *NIPS*, 2016.
- [40] Moritz Wolter and Angela Yao. Complex gated recurrent neural networks. In *NIPS*, 2018.
- [41] Wei Zuo, Yang Zhu, and Lilong Cai. Fourier-neural-network-based learning control for a class of nonlinear systems with flexible components. *IEEE transactions on neural networks*, 20(1):139–151, 2008.